Pore Formation in a Binary Giant Vesicle Induced by Cone-Shaped Lipids

Yuka Sakuma,[†] Takashi Taniguchi,[‡] and Masayuki Imai[†*]
[†]Department of Physics, Ochanomizu University, Bunkyo, Tokyo, Japan; and [‡]Graduate School of Science and Engineering, Yamagata University, Yonezawa, Yamagata, Japan

ABSTRACT We have investigated shape deformations of binary giant unilamellar vesicles (GUVs) composed of cone- and cylinder-shaped lipids. By coupling the spontaneous curvature of lipids with the phase separation, we demonstrated pore opening and closing in GUVs. When the temperature was set below the chain melting transition temperature of the cylinder-shaped lipid, the GUVs burst and then formed a single large pore, where the cone shape lipids form a cap at the edge of the bilayer to stabilize the pore. The pore closed when we increased the temperature above the transition temperature. The pore showed three types of shapes depending on the cone-shaped lipid concentration: simple circular, rolled-rim, and wrinkled-rim pores. These pore shape changes indicate that the distribution of the cone- and cylinder-shaped lipids is asymmetric between the inner and outer leaflets in the bilayer. We have proposed a theoretical model for a two-component membrane with an edge of bilayer where lipids can transfer between two leaflets. Using this model, we have reproduced numerically the observed shape deformations at the rim of pore.

INTRODUCTION

Deformations of cell membranes, such as fusion, adhesion, budding, and pore formation, play important roles in the maintenance of living cell systems. In cell systems, the membrane deformations are managed by complex interplays between membrane proteins and lipids. It is hypothesized that one role of the membrane proteins is to introduce a local spontaneous curvature by interacting with the membranes (1), although the relationship between the local spontaneous curvature and the shape deformations has not been demonstrated. In this context, we have been investigating the shape deformations of giant unilamellar vesicles (GUVs) induced by the local spontaneous curvature of the membranes (2,3).

We have introduced the local spontaneous curvature by mixing two types of lipids having different geometries. If a lipid has bulky hydrocarbon chains and a small headgroup (e.g., an inverse-cone-shaped lipid as shown in Fig. 1 *a*), the lipid monolayer has a tendency to bend toward the side of the headgroup, which is defined as a negative spontaneous curvature. Similarly, a lipid having small hydrocarbon chains and a large headgroup (e.g., a cone-shaped lipid as shown in Fig. 1 *b*) tends to bend the lipid monolayer toward the side of the tails, which is defined as a positive spontaneous curvature. A lipid that prefers to form a flat monolayer is referred to as a cylinder-shaped lipid (Fig. 1 *c*). For binary membranes composed of immiscible lipids having different geometries, the local spontaneous curvature and the bending modulus depend on the local composition of the membrane. The heterogeneity of a membrane coupled with the line energy at the phase boundary brings new shape deformation branches. For example, the binary GUV composed of the inverse-cone-shaped lipids and cylinder-shaped lipids might show adhesion through the domains rich in inverse-cone-shaped lipids by forming an hourglass-like interbilayer structure called a stalk (4,5) (see our Fig. 1 *a*).

In our previous experiments, we have achieved the adhesion of GUVs, which was caused by the coupling of negative spontaneous curvature of lipid to the membrane phase separation in binary systems of dipalmitoyl-phosphoethanolamine (DPPE/ 16:0-16:0 PE) and dioleoyl-phosphocholine (DOPC, 18:1-18:1 PC) or diphytanoyl-phosphocholine (DPhPC/ 16:0(3me, 7me, 11me, 15me)-16:0 (3me, 7me, 11me, 15me) PC) and dipalmitoyl-phosphocholine (DPPC/ 16:0-16:0 PC)(2). DPPC has a small headgroup and DPhPC has bulky tails, such that the lipids take the shape of inverse-cones, whereas DOPC and DPPC take the shape of cylinders. Fig. 1 *a* shows adhering DPhPC/DPPC binary GUVs. A fluorescent lipid transfer experiment strongly implied that a stalk formed between adhering vesicles (2).

We have also previously shown that for the case of ternary GUVs composed of two types of immiscible cylinder-shaped lipids (DOPC and DPPC) and cholesterol, the shape of the GUVs is governed by the line energy between coexisting liquid-ordered and liquid-disordered phases. The GUVs produce various budding phenomena (3,6) (see Fig. 1 *c*), which resembles endocytosis (inside budding) and fission (outside budding) in cell membranes. The inside and outside buddings of GUVs were realized in the DPPC/DOPC/cholesterol ternary GUV system by controlling the area/volume ratio of the GUV (see Fig. 1 *c* and (3)).

In this study, we focus on the shape deformations of binary GUVs composed of cone-shaped lipids (1,2-dihexanoyl-*sn*-glycero-3-phosphocoline, 6:0-6:0 PC; DHPC) and cylinder-shaped lipids (DPPC). In water, DHPC molecules form prolate micelles with the radius of minor axis, ~1.35 nm,

Submitted August 28, 2009, and accepted for publication March 29, 2010.

*Correspondence: imai@phys.ocha.ac.jp

Takashi Taniguchi's present address is Department of Chemical Engineering, Kyoto University, Kyoto 615-8510, Japan.

Editor: Reinhard Lipowsky.

0006-3495/10/07/0472/8 $2.00

doi: 10.1016/j.bpj.2010.03.064

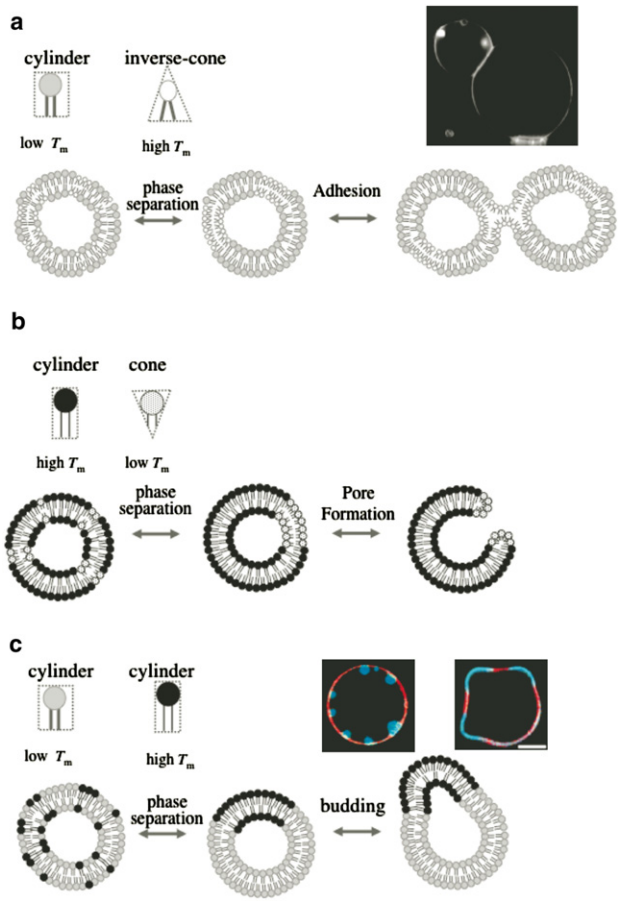

FIGURE 1 Schematic representations for shape deformations of binary GUVs coupled with spontaneous curvature of lipids. (*a*) Adhesion of binary GUVs composed of inverse-cone-shaped lipids and cylinder-shaped lipids. A photo shows a cross-sectional image of adhering DPhPC/DPPC binary GUVs (2). (*b*) Pore formation of binary GUVs composed of cone-shaped lipids and cylinder-shaped lipids. (*c*) Budding of GUVs composed of two types of cylinder-shaped lipids. Photos show cross-sectional images of inside budding (*left*) and outside budding (*right*) of GUVs observed in DPPC/DOPC/cholesterol ternary GUV system (3). Red and blue parts (color online, *light gray* and *dark gray* parts in print) indicate liquid-disordered phase and liquid-ordered phase, respectively.

and radius of major axis, ~2.5 nm (7), indicating the positive spontaneous curvature of 1/1.35~1/2.5 nm^{-1}. The binary GUV shows a phase separation between a solid phase rich in DPPC and a liquid phase rich in DHPC at all intermediate temperatures between the chain melting transition temperatures. The segregated cone-shaped lipids might form a cap at the edge of the bilayer (8,9), which may stabilize the pore (see Fig. 1 *b*).

MATERIALS AND METHODS

Commercial reagents

The cone-shaped lipids, 1,2-dihexanoyl-*sn*-glycero-3-phosphocholine (DHPC/ 6:0-6:0 PC), and three types of the cylinder-shaped lipids, 1,2-dipentadecanoyl-*sn*-glycero-3-phosphocholine (15:0-15:0 PC), DPPC, and 1,2-distearoyl-*sn*-glycero-3-phosphocholine (DSPC/ 18:0-18:0 PC) were purchased from Avanti Polar Lipids (Alabaster, AL). Texas Red 1,2-dihexanoyl-*sn*-glycero-3-phosphoethanolamine (TR-DHPE) was obtained from Molecular Probes (Eugene, OR) and used as a dye for membranes.

GUVs preparation

The GUVs were prepared by a gentle hydration method (10,11). To begin, we dissolved the prescribed amount of phospholipids in 10 μL of chloroform (10 mM). To dye GUVs, TR-DHPE was added to the solution with molar concentration of 0.36%. The solvent was evaporated in a stream of nitrogen gas and the obtained lipid film was kept under vacuum for one night to remove the remaining solvent completely. The dried lipid film was prewarmed at 60°C, and then the sample was hydrated with 1 mL of pure water of 60°C. During the hydration process, the lipid films spontaneously form GUVs with diameters of 10–40 μm. All the experiments in this study were performed using pure water without salt.

Pore formation experiment

We prepared binary GUVs composed of DHPC and DPPC with various DHPC concentrations, 0.01, 0.03, 0.1, 0.3, 0.5, 1.0, 2.0, 3.0, 4.0, 5.0, 10.0, 12.0, 20.0, 30.0, 40.0, 50.0, 60.0, and 80.0 mole %. The binary GUV suspension was put on a glass plate with a silicon rubber spacer having the thickness of 0.5 mm, and then sealed with a cover glass immediately. This sample cell was set on the temperature control stage (model No. FP90; Mettler-Toledo International, Mississauga, Ontario, Canada), which controlled the sample temperature from 10 to 60°C with ± 0.1°C accuracy. The chain melting transition temperatures of DPPC and DHPC measured by differential scanning calorimetry (EXSTAR DSC6000; SII Nano Technology, Chiba, Japan) were $T_m^{DPPC} = 41$°C and $T_m^{DPPC} = -46$°C, respectively.

To avoid phase separation before the observation, we kept the sample temperature above T_m^{DPPC}. We decreased the temperature from the one-phase region (60°C) to the coexisting solid-liquid two-phase region (10°C) and then increased the temperature to the homogeneous one-phase region at a rate of 1.0°C/min. Both processes were followed using a fluorescence microscope (Axioskop 40; Carl Zeiss, Jena, Germany) with a charge-coupled device camera (Axio Cam MRm; Carl Zeiss) and an inverted confocal fluorescence microscope for three-dimensional imaging (LSM 5 Pascal; Carl Zeiss). The three-dimensional images for pot GUVs were constructed using ~50 slice images with 0.66-μm thickness and a scan rate of 100 ms/slice. To avoid photooxidation, we paid special attention to minimize the exposure time of light. We performed similar experiments for the 15:0 PC/DHPC and DSPC/DHPC systems.

RESULTS AND DISCUSSION

Shape diagram of binary GUVs composed of cylinder-shaped and cone-shaped lipids

In the one-phase region above T_m^{DPPC}, binary GUVs show an homogeneous spherical shape with a radius of 10~30 μm. Contrast variation experiments with small-angle neutron scattering (12) using deuterated DPPC and hydrogenated DHPC revealed that both lipids are mixed homogeneously at the molecular scale. Decreasing the temperature below T_m^{DPPC}, the spherical GUVs burst at 38.9°C, and the inner solution was released from the vesicle as shown by an arrow in Fig. 2 *a*. At temperatures between $T_m^{DPPC} = 41$°C and the bursting temperature of 38.9°C, the lipids are likely phase-separated into a DPPC-rich solid and a DHPC-rich liquid phases (13), although we could not detect domains on binary

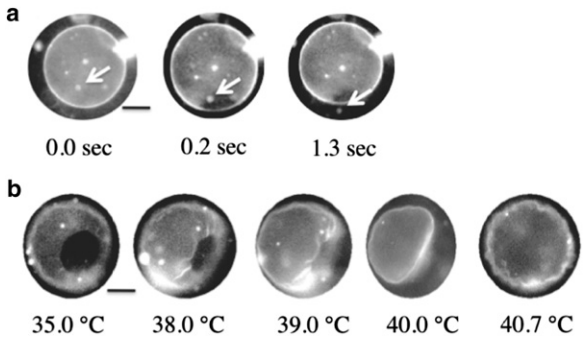

FIGURE 2 Snapshots of the (*a*) formation (time evolution at 38.9°C) and (*b*) closing (temperature dependence) of a pore in a simple pot-GUV with DPPC/DHPC = 99:1. When a pore opens, a small vesicle is ejected through the pore as shown by arrows in panel *a*. Scale bar is 5 μm.

GUVs by fluorescence microscopy. Our small-angle neutron scattering measurements revealed that the surface area of a pure DPPC vesicle below T_m^{DPPC} was ~78% of the area of a vesicle above T_m^{DPPC} (12), which agrees with the reported value of 72% (14). This decrease in the surface area increases the inner pressure of the vesicle, resulting in the fracture of membrane (15). After bursting, a spherical GUV immediately transformed into a pot-shaped GUV (pot-GUV) with a single pore and the pore was stable below T_m^{DPPC}. It has been reported that formation of micrometer-sized pores in GUVs can be achieved by the addition of specific detergents (16,17). For the detergent-induced pore formation, the detergent extracts the lipids from the membrane to the surrounding solvent phase (solubilization). Inasmuch as the vesicle keeps the volume constant during the solubilization, this decrease of the number of lipid molecules increases the surface tension of the vesicle. Then the liposome discharges water molecules from its interior by the pore formation. After the release of the inner pressure, the line tension at the rim forces the pore to close up, i.e., the pore is unstable and transient (18,19). For the pore formation in the binary GUVs composed of cone- and cylinder-shaped lipids, the segregated cone-shaped lipids cap the edge of the bilayer at the rim of the pore (8,9); this decreases the line tension at the rim. DPPC in the gel state then solidifies the main body of the GUV. These effects stabilize the pore in $T < T_m^{DPPC}$.

A unique feature of the pore formation in this study is that the pore opening and closing could be controlled by the temperature. When we increased the temperature of the pot-GUV to the one-phase region, the pore started to shrink at ~37°C and simultaneously, radial wrinkles appeared around the pore (Fig. 2 *b*). The wrinkles grew as the pore size continued to decrease. At 40.0°C, which is just below T_m^{DPPC}, the pore closed with the wrinkles, and the vesicle showed a deformed shape (Fig. 2 *b*). The deformed GUV recovered its spherical shape as a result of the chain melting, although it had a flaccid shape, i.e., the recovered vesicle had larger excess area (surface area/volume ratio of the vesicle) than the original spherical vesicle. When we decreased the temperature of the recovered GUV, we could not observe definite pore formation, because the excess area allowed the surface area of the GUV to decrease without increasing the inner pressure of the vesicle.

The observed morphologies of pot-GUVs can be classified into three types depending on the DHPC mole fraction *m* as shown in Fig. 3, in which we show the typical two- and three-dimensional, and cross-sectional confocal microscope images. At each concentration (designated by *arrows*), we examined ~100 GUVs and the fraction of each vesicle type is shown on the vertical axis. At the low DHPC concentrations ($0.1 < m < 1\%$), the normal spherical GUV and simple pot-GUV coexisted. The simple pot-GUV had a smooth circular pore with a diameter of 2–5 μm.

When the DHPC concentration increased, the pot-GUVs show shape deformations. For $0.5 < m < 8\%$ the membrane peripheral to the simple pore changed to the rolled-rim shape. The cross-section image in Fig. 3 shows that the membrane at the rim rolled up. The rolled rim was stable below T_m^{DPPC}. The formation of the rolled rim implies an asymmetric distribution of the cone-shaped lipids between the upper and the lower leaflets. As the flip-flop rate of lipids in the absence of cholesterol is <~500 min^{-1} (20), here we ignored the effect of flip-flop motion between the upper and the lower leaflets.

A plausible explanation of the rolled-rim formation is as follows. The DHPC cap at the edge of the bilayer forms bridges between the inner and outer leaflets and the

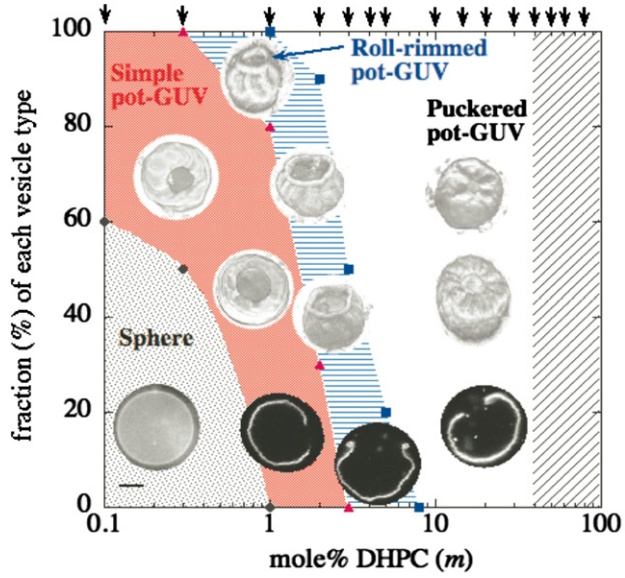

FIGURE 3 Morphology diagram of DHPC/DPPC pot-GUVs at 25°C as a function of DHPC mole fraction *m*, with typical fluorescence microscope images (the scale bar indicates 5 μm). The vertical axis represents the fraction of each morphology and arrows at upper axis indicate examined DHPC mole %. Circles, triangles, and squares indicate observed borders between spheres/simple pot-GUVs, simple/roll-rimmed pot-GUVs, and roll-rimmed/puckered pot-GUVs, respectively. In the shaded region, the binary lipids could not form GUVs.

remaining cone-shaped lipids around the rim migrate toward a convexly deformed leaflet (note that the hydrophilic part has a larger area than the hydrophobic part) through the fluid cap, due to the geometrical preference. The resultant asymmetric distribution of cone-shaped lipids between inner and outer leaflets causes the local spontaneous curvature, which bends the membrane to form the rolled rim. The detailed relationship between distribution of cone-shaped lipids in the bilayer and the membrane deformation, based on our simulation, will be discussed in Theoretical Model for Shape Deformation of Pot-GUV, below. Here, however, we have to investigate the shape behavior experimentally in more detail, because lipid traffic, in relation to its molecular geometries (21–23), is a central issue of cellular organelle homeostasis.

For $2 < m < 40\%$, the pot-GUVs showed a puckered-rim shape. The membrane around the pore bent toward the inside of the vesicle slightly and had radial wrinkles (shown in Fig. 3). The wrinkling sometimes had a periodic nature in the azimuthal direction, although individual GUVs possessed different wavelengths. The time evolution of the wrinkling showed that after bursting, the pore size of the puckered pot-GUV decreased to the stable pore size, which resulted in radial wrinkles (similar to the pore-closing process seen in Fig. 2 *b*). During the process of shrinking, the elastic membrane around the pore is stretched in the radial direction and compressed in the tangential direction—which is responsible for the periodic wrinkle formation (24,25). Whether shrinking of the pore occurs, depends on the composition of the membrane.

We confirmed similar pore formation for other pairs of cylinder-shaped lipids and cone-shaped lipids (i.e., the 18:0 PC/DHPC and 15:0 PC/DHPC mixtures); however, with these combinations, the pore opening temperature increases with an increase in the acyl chain length. The 15:0 PC/DHPC GUVs had a pore-opening temperature of ~29°C ($T_m^{15:0PC} = 34°C$), and the 18:0 PC/DHPC GUVs had a pore-opening temperature of ~50°C ($T_m^{DPPC} = 54°C$).

In the next subsection, supported by the results presented above, we hypothesize that phase separation between cylinder-shaped lipids and cone-shaped lipids is responsible for pore formation.

Theoretical model for shape deformation of pot-GUV

Here we propose a model to describe the shape deformations of the DHPC/DPPC binary vesicle after forming a single pore. We investigate whether the formation of rolled rim can be explained by a model that is based on the assumption of interleaflet lipid transfer, wherein lipids in the inner and outer leaflets can cross between the leaflets through the edge of the pore. In our experiments, although one of the separated phases passes into the gel state after the system reached a well phase-separated state, we neglected the shear elastic energy contribution inasmuch as we focus on the shape deformation and phase separation in the fluid state before it reaches the gel state. A position on the membrane is expressed by $\mathbf{r}(\{u\}, t)$, where $\{u\} \equiv \{u_1, u_2\}$ indicate the parameters that describe the coordinate on the membrane. The local compositions of DHPC in the inner leaflet and the one in the outer leaflet are given by $\phi_{\mathrm{DHPC}}^{(\mathrm{in})}(\mathbf{r}, t)$ and $\phi_{\mathrm{DHPC}}^{(\mathrm{out})}(\mathbf{r}, t)$, respectively. The local incompressibility condition

$$\phi_{\mathrm{DHPC}}^{(\mathrm{in/out})}(\mathbf{r}, t) + \phi_{\mathrm{DPPC}}^{(\mathrm{in/out})}(\mathbf{r}, t) = 1,$$

holds for both the inner and outer leaflets. After forming a single pore, the total free energy of the vesicle with coexisting fluid domains is given by $F = F_{\mathrm{b}} + F_{\mathrm{mix}} + F_{\mathrm{rim}}$. F_{b} is the bending energy given by

$$F_{\mathrm{b}} = \int \left[\frac{\kappa}{2} H^2 - \kappa H_0 H\right] dS, \tag{1}$$

where $H/2$ is the mean curvature and $H_0/2$ is the local spontaneous curvature that is proportional to the local composition difference $\delta\phi_{\mathrm{DHPC}}(\mathbf{r}, t) = \phi_{\mathrm{DHPC}}^{(\mathrm{out})}(\mathbf{r}, t) - \phi_{\mathrm{DHPC}}^{(\mathrm{in})}(\mathbf{r}, t)$ between the inner and outer leaflet, as

$$H_0(\mathbf{r}) = \frac{\Lambda}{\kappa} \delta\phi_{\mathrm{DHPC}}(\mathbf{r}, t),$$

where Λ is a positive constant. F_{mix} is the mixing free energy including the line energy at domain boundaries, in each of two leaflets,

$$F_{\mathrm{mix}} = \sum_{\mathrm{X=in,out}} \int \left[\frac{b}{8}\left(\nabla(\phi_{\mathrm{DHPC}}^{(\mathrm{X})} - \phi_{\mathrm{DPPC}}^{(\mathrm{X})})\right)^2 + f\left(\phi_{\mathrm{DHPC}}^{(\mathrm{X})}, \phi_{\mathrm{DPPC}}^{(\mathrm{X})}\right)\right] dS, \tag{2}$$

where

$$f\left(\phi_{\mathrm{DHPC}}^{(\mathrm{X})}, \phi_{\mathrm{DPPC}}^{(\mathrm{X})}\right) = \phi_{\mathrm{DHPC}}^{(\mathrm{X})} \ln \phi_{\mathrm{DHPC}}^{(\mathrm{X})} + \phi_{\mathrm{DPPC}}^{(\mathrm{X})} \ln \phi_{\mathrm{DPPC}}^{(\mathrm{X})} + \chi \phi_{\mathrm{DHPC}}^{(\mathrm{X})} \phi_{\mathrm{DPPC}}^{(\mathrm{X})},$$

and b is a parameter to control the line energy at domain boundaries and χ describes the affinity between DHPC and DPPC. F_{rim} is the energy of rim of membrane with a pore,

$$F_{\mathrm{rim}} = \int_{\partial S} \left[\Gamma_0 + \Gamma_1\left(\phi_{\mathrm{DHPC}}^{(\mathrm{in})}(\mathbf{r}_{\mathrm{e}}) + \phi_{\mathrm{DHPC}}^{(\mathrm{out})}(\mathbf{r}_{\mathrm{e}})\right)\right] d\mathbf{r}_{\mathrm{e}}, \tag{3}$$

where $\mathbf{r}_{\mathrm{e}}$ denotes a position on the rim and the integral is performed along the perimeter of the pore, and Γ_0 and Γ_1 are constants. Because the positive spontaneous curvature lipid, DHPC, prefers the capped rim, Γ_1 is negative. For the vesicle with a pore, the area difference energy (26) can be omitted, as the lipids can be exchanged through the capped rim at the pore of the vesicle. The dynamics of shape deformation is assumed to be described by

$$\frac{\partial\, \mathbf{r}(\{u\},t)}{\partial t} = -L\frac{\delta\, F}{\delta\, \mathbf{r}(\{u\},t)}, \tag{4}$$

where L is a damping coefficient. We used a local Lagrange multiplier $\gamma(\{u\})$ to guarantee the local incompressibility condition for membrane area (27). It should be noted that the pore formation breaks the conservation law of vesicle volume and the mass conservation of each component in each inner and outer leaflet. The time evolutions of the local composition of DHPC in the inner and outer leaflet are described by

$$\frac{\partial\phi^{(\mathrm{in})}_{\mathrm{DHPC}}(\mathbf{r},t)}{\partial t} = L_0\Delta_{\mathrm{LB}}\mu^{(\mathrm{in})}(\mathbf{r}) - L_1\big(\mu^{(\mathrm{in})}(\mathbf{r}_\mathrm{e}) - \mu^{(\mathrm{out})}(\mathbf{r}_\mathrm{e})\big)\delta_{\mathbf{r}\mathbf{r}_\mathrm{e}}, \tag{5}$$

$$\frac{\partial\phi^{(\mathrm{out})}_{\mathrm{DHPC}}(\mathbf{r},t)}{\partial t} = L_0\Delta_{\mathrm{LB}}\mu^{(\mathrm{out})}(\mathbf{r}) - L_1\big(\mu^{(\mathrm{out})}(\mathbf{r}_\mathrm{e}) - \mu^{(\mathrm{in})}(\mathbf{r}_\mathrm{e})\big)\delta_{\mathbf{r}\mathbf{r}_\mathrm{e}}, \tag{6}$$

where L_0 and L_1 are transport coefficients, Δ_{LB} is the Laplace-Beltrami operator, $\mu^{(\mathrm{x})}$ is the chemical potential defined by $\mu^{(\mathrm{x})} = \delta F/\delta\phi^{(\mathrm{x})}_{\mathrm{DHPC}}(\mathbf{r})$ (X stands for in or out), and $\delta_{\mathbf{r}\mathbf{r}'}$ is the Krönecker's delta. The first terms on the right side of Eqs. 5 and 6 describe diffusions of DHPC lipids driven by the thermodynamic force and the second terms express the exchange rates of DHPC lipids between the inner and outer leaflet through the capped rim. So far, effects of the line tension (27–34), the local spontaneous curvature (27–33), and the local bending rigidity (31–33) have been taken into account to investigate the phase diagram of a two-component vesicle theoretically. Furthermore, the morphology of the phase-separated vesicle has been addressed by a Monte Carlo simulation (35) and a dissipative particle dynamics simulation (36–38). Although the equilibrium shapes of two-component vesicle have been intensively investigated both theoretically and numerically as mentioned above, none of these investigations have reported a membrane with a rolled rim. Therefore, to describe the dynamics of shape deformation and phase separation of a two-component vesicle with a single pore, and to understand the reason why the membrane can be rolled near the rim after forming a pore, we consider the model described by Eqs. 1–6. This model is an extension of the previous continuum model (27–34,39) of a two-component vesicle. The highlight of our newly proposed model is the incorporation of two new contributions: 1), transfer of lipids through the cap at the rim (Eqs. 5 and 6) and 2), stabilization of the pore by the cone-shaped lipid (Eq. 3), into the previous continuum model.

Here we consider an axisymmetric spherical vesicle with a single pore (as shown in Fig. 4 *c1*) that is assumed to be in the just-after-bursting state, and numerically calculate the shape deformation and phase separation using the model of a two-component membrane given in Eqs. 4–6. Because

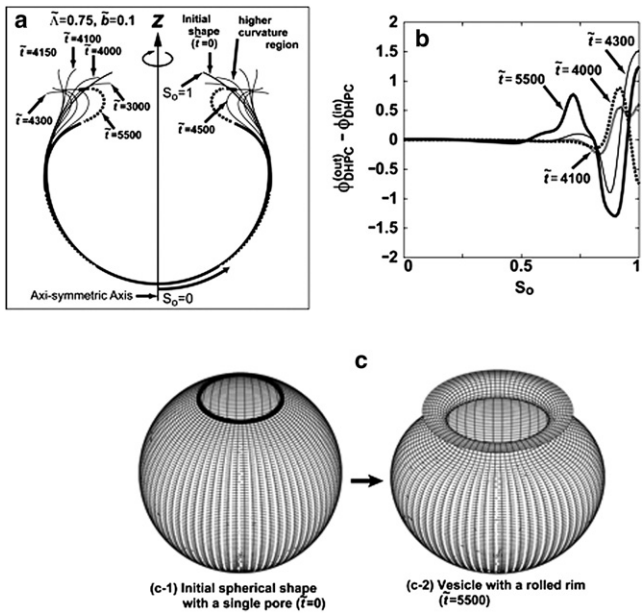

FIGURE 4 (*a*) Shape deformations for the cases $\tilde{\Lambda} = 0.75$ and $\tilde{b} = 0.1$ at scaled times $\tilde{t}$ = 3000, 4000, 4100, 4150, 4300, 4500, and 5500 from the initial spherical vesicle ($\tilde{t}$ =0) with a single pore. In the shape at $\tilde{t}$ =5500, the region with $\delta\phi_{\mathrm{DHPC}}$ (S_o,t) > 0 is drawn by the solid line and the one with $\delta\phi_{\mathrm{DHPC}}$ (S_o,t) < 0 is drawn by the dotted line. (*b*) The area fraction difference in DHPC between inner and outer leaflets $\delta\phi_{\mathrm{DHPC}}(S_o, t)$ at $\tilde{t}$ = 4000, 4100, 4300, and 5500 as functions of S_o defined as the contour length measured from the intersection point of the vesicle with the z axis at $\tilde{t} = 0$. (*c*) The axisymmetric three-dimensional figure of the initial shape ($\tilde{t} = 0$) and the vesicle with a rolled rim at $\tilde{t}$ = 5500 in panel *a*.

our model is based on the continuum hypothesis to describe the vesicle and hence it is too hard to treat the burst process by our present model, we performed all the simulations using a vesicle with a single pore as an initial state. In the initial states, we assumed that DPPC and DHPC are homogeneously distributed both in the outer and inner leaflets, i.e., constant $\overline{\phi}^{(\mathrm{out})}_{\mathrm{DHPC}}$ and $\overline{\phi}^{(\mathrm{in})}_{\mathrm{DHPC}}$. We set the temperature to the bare critical temperature of phase separation (see Note following); it corresponds to

$$\Delta\chi = \chi - \chi_c = 0(\chi_c = 2),$$

in Eq. 2. The other parameters we used are

$$\kappa/k_\mathrm{B}T = 5,$$

$$r_0/\ell_0 \cong 35,$$

$$\tilde{\Lambda} = \Lambda\ell_\mathrm{o}/k_\mathrm{B}T = 0.75,$$

$$\tilde{L} = L/L_0 = 1.0,$$

$$\tilde{L}_1 = L_1\ell_0^2/L_0 = 0.01,$$

$$\tilde{\Gamma}_0 = \Gamma_0\ell_\mathrm{o}/k_\mathrm{B}T = 0.15, \text{ and}$$

$$\tilde{\Gamma}_1 = \Gamma_1\ell_\mathrm{o}/k_\mathrm{B}T = -0.10,$$

where r_0 is the radius of initial spherical shape and ℓ_0 is a unit of length.

Note that the point ($\overline{\phi}^{(\mathrm{in})}_{\mathrm{DHPC}} = \overline{\phi}^{(\mathrm{out})}_{\mathrm{DHPC}} = 0.5$, $\delta\chi = \chi - \chi_c = 0$) in the phase diagram (see Fig. 5) is not the true critical point, but is instead the bare critical point, inasmuch as χ_c is the value of the χ-parameter at the critical point in bulk (i.e., χ_c is determined only by using Eq. 2; in other words, without shape deformation). In closed two-component vesicles, the value of the χ-parameter that gives the critical point is shifted from χ_c to a lower value ($\chi_c^{(\mathrm{true})} = \chi_c - 2\Lambda^2/\kappa$) by the local spontaneous term (the second term in the integrand) in Eq. 1. (The shift of critical temperature owing to the local spontaneous curvature was reported in (30).)

First, in Fig. 4 we show a result of simulation for the case of $\overline{\phi}^{(\mathrm{in})}_{\mathrm{DHPC}} = 0.35$ and $\overline{\phi}^{(\mathrm{out})}_{\mathrm{DHPC}} = 0.35$ —a typical case in which the vesicle deforms from a spherical vesicle with a single pore to the one with a rolled rim by the coupling of vesicle shape to an intramembrane phase separation. Fig. 4 *a* shows time-sequential snapshots of the vesicle deformation with a phase separation. The axisymmetric shape at the dimensionless time $\tilde{t} = 5500$ is drawn by a dotted line where $\delta\phi_{\mathrm{DHPC}}$ (**r**,*t*) is negative, and by the solid line where $\delta\phi_{\mathrm{DHPC}}$ (**r**,*t*) is positive. The corresponding three-dimensional figure to the shape at $\tilde{t} = 5500$ in Fig. 4 *a* is depicted in Fig. 4 *c2*. In Fig. 4 *b*, $\delta\phi_{\mathrm{DHPC}}$ (S_o,*t*) at $\tilde{t} = 4000$, $\tilde{t} = 4100$, and $\tilde{t} = 5500$ are plotted as functions of a material coordinate S_o defined as the contour length measured from the intersection point of the vesicle with the *z* axis at $\tilde{t} = 0$ (see Fig. 4 *a* for S_o).

As seen from Fig. 4, *a* and *c* (also seen later from the vesicle shapes shown in Fig. 5), our model well reproduces the vesicle shape with a rolled rim. The mechanism of formation of rolled rim is as follows. In the initial stage ($\tilde{t} < 4000$), the vesicle shape is dominated by the positive line tension of the rim and therefore the vesicle deforms to reduce the length of rim, which results in the formation of a higher curvature region near the rim (as indicated by an *arrow* for the shape at $\tilde{t} = 4000$ in the Fig. 4 *a*). Then at the higher curvature region, $\delta\phi_{\mathrm{DHPC}}$ (S_o,*t*) increases with time because of the curvature-composition coupling in Eq. 1. After the initial stage ($\tilde{t} \geq 4100$), a depletion region of $\delta\phi_{\mathrm{DHPC}}$ (S_o,*t*) at $\sim S_o \cong 0.8$ starts to form and grow (see Fig. 4 *b*), while the depletion of $\delta\phi_{\mathrm{DHPC}}$ (S_o,*t*) near the rim is compensated by DHPC transported from the inner leaflet through the capped rim. Finally the depletion at $\sim S_o \cong 0.8$ grows and shifts to the edge direction, which results in a composition profile similar to that at $\tilde{t} = 5500$ in Fig. 4 *b*. The resultant depletion region of $\delta\phi_{\mathrm{DHPC}}$ (S_o,*t*) at $\sim S_o \cong 0.8$~0.9 brings a negative spontaneous curvature at the position by means of the coupling term in Eq. 1. The negative spontaneous curvature is the origin of the formation of the rolled rim. As seen from the graph at $\tilde{t} = 5500$ in Fig. 4 *a* (*solid line*), in a region close to the rim, the area fraction of DHPC in the outer leaflet

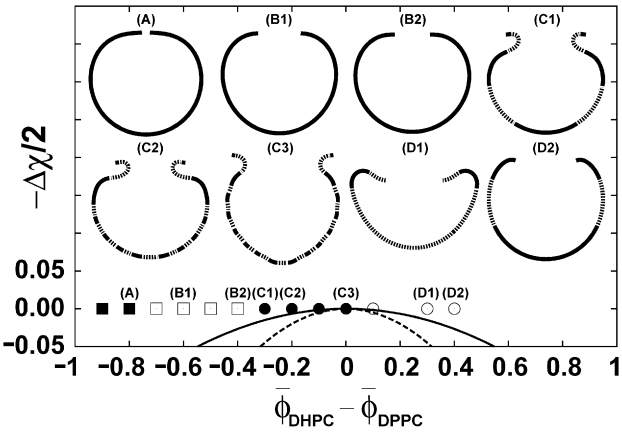

FIGURE 5 Initial composition dependence of shape deformation of a vesicle with a single pore just on the bare critical temperature ($\Delta\chi = 0$). The solid line and dashed line below $\Delta\chi = 0$ represent binodal and spinodal lines of phase separation in bulk, respectively. Symbols in the phase diagram—the solid square, open square, solid circle, and open circle—mean that a vesicle after bursting will becomes a closed vesicle, an open vesicle with a simple rim, a vesicle with a rolled rim, and an open vesicle with a rim which bends toward inside, respectively. Typical shapes obtained at positions specified by four different symbols are also shown for panels *A–D*. For panels *C1–C3*, *D1* and *D2*, the region with $\delta\phi_{\mathrm{DHPC}} > 0$ is drawn by a solid line and the one with $\delta\phi_{\mathrm{DHPC}} < 0$ is drawn by a dotted line, but the shapes in panels *A*, *B1*, and *B2* are drawn only by solid line, because the phases are not well separated.

$\phi^{(\mathrm{out})}{}_{\mathrm{DHPC}}$ (**r**,*t*) becomes larger than that in the inner leaflet $\phi^{(\mathrm{in})}{}_{\mathrm{DHPC}}$ (**r**,*t*). This is because DHPC geometrically prefers the positive curvature region, which results in a positive local spontaneous curvature. In addition, next to the DHPC excess region in the outer leaflet, a depletion region of DHPC in the outer leaflet is formed (indicated by *dotted line* in Fig. 4 *a*), which yields a negative spontaneous curvature and the rim-rolled membrane shown in Fig. 4, *a* and *c2*. In Fig. 5, we show the composition dependence of shape deformation on the line of $\Delta\chi = 0$ (see Note above), where the solid-square, open-square, solid-circle, and open-circle symbols stand for closed vesicles, open vesicles, vesicles with a rolled rim, and open vesicles with a rim bending toward the inside, respectively.

The qualitative tendency of phase diagram shown in Fig. 5 is in good agreement with the experimentally obtained diagram in Fig. 3 except for a wrinkled rim. It should be noted that as this model is valid for the fluid state, the wrinkling is beyond the application of this model. In the region of the solid and open squares, positive line tension of the rim is dominant and therefore the vesicle in the region deforms to reduce the length of the rim. In the region of the solid and open circles, the competition mainly between the line tension term of the rim and the local spontaneous curvature term in free energy plays an important role in determining unique vesicle shapes and composition distribution. Thus, the exchange of lipids through the capped rim and the coupling of the local membrane composition with the shape around the rim produce a local asymmetry between the inner and

outer leaflet—resulting in the formation of a rolled-rim vesicle morphology.

CONCLUSIONS

In the binary vesicle composed of cone- and cylinder-shaped lipids, the main chain transition of cone-shaped lipids reduces the surface area, which results in the pore formation. The segregated cone-shaped lipids form the cap at the edge of bilayer and the cylinder-shaped lipid in gel state solidifies the main body of the GUV. These effects stabilize the pore below the main chain transition temperature. In contrast to the pore formation induced by the addition of the detergents, a unique feature of this system is that the pore formation is controlled by changing the temperature. At pore formation, the binary GUVs showed different morphologies at the rim of the pore, i.e., smooth, rolled, or wrinkled rim, which were dependent upon the concentration of the cone-shaped lipid, and indicated the asymmetric distribution of the cone-shaped lipid in the bilayer. By incorporating two contributions (transfer of lipids through the cap at the rim and stabilization of the pore by the cone-shaped lipid) into the previous continuum model, we reproduced the observed shape deformations at the rim of pore numerically. The exchange of lipids through the capped rim and the coupling of the local composition of the membrane with the membrane curvature bring about a local composition of asymmetry between the inner and outer leaflet, which causes vesicle shape deformations such as the formation of a rolled rim.

This study clearly demonstrates the relationship between the local spontaneous curvature and the shape deformation of vesicles. We believe that our results provide new insight into the physical basis of the shape deformation of cellular membranes.

We thank Prof. Toshihiro Kawakatsu (Tohoku University) for valuable discussions.

This work was supported by KAKENHI (Grant-in-Aid for Scientific Research) on the Priority Area ''Soft Matter Physics'' from the Ministry of Education, Culture, Sports, Science and Technology of Japan and Grant-in-Aid for Scientific Research (B) No. 19340118 from Japan Society for the Promotion of Science. Y.S. thanks the Japan Society for the Promotion of Science, Grant-in-Aid, for support by its JSPS Fellows grant (No. 20-2802).

REFERENCES

1. Zimmerberg, J., and M. M. Kozlov. 2006. How proteins produce cellular membrane curvature. *Nat. Rev. Mol. Cell Biol.* 7:9–19.
2. Sakuma, Y., M. Imai, …, S. Komura. 2008. Adhesion of binary giant vesicles containing negative spontaneous curvature lipids induced by phase separation. *Eur. Phys. J. E Soft Matter*. 25:403–413.
3. Yanagisawa, M., M. Imai, and T. Taniguchi. 2008. Shape deformation of ternary vesicles coupled with phase separation. *Phys. Rev. Lett.* 100:148102.
4. Gingell, D., and I. Ginsberg. 1978. Problems in the physical interpretation of membrane interaction and fusion. *In* Membrane Fusion. G. Poste and G. L. Nicholson, editors. Elsevier, Amsterdam, The Netherlands.
5. Yang, L., and H. W. Huang. 2002. Observation of a membrane fusion intermediate structure. *Science*. 297:1877–1879.
6. Baumgart, T., S. T. Hess, and W. W. Webb. 2003. Imaging coexisting fluid domains in biomembrane models coupling curvature and line tension. *Nature*. 425:821–824.
7. Lipfert, J., L. Columbus, …, S. Doniach. 2007. Size and shape of detergent micelles determined by small-angle x-ray scattering. *J. Phys. Chem. B*. 111:12427–12438.
8. Sanders, C. R., and J. P. Schwonek. 1992. Characterization of magnetically orientable bilayers in mixtures of dihexanoylphosphatidylcholine and dimyristoylphosphatidylcholine by solid-state NMR. *Biochemistry*. 31:8905–9989.
9. Katsaras, J., R. L. Donaberger, …, R. S. Prosser. 1997. Rarely observed phase transitions in a novel lyotropic liquid crystal system. *Phys. Rev. Lett.* 78:899–902.
10. Reeves, J. P., and R. M. Dowben. 1969. Formation and properties of thin-walled phospholipid vesicles. *J. Cell. Physiol.* 73:49–60.
11. Needham, D., and E. Evans. 1988. Structure and mechanical properties of giant lipid (DMPC) vesicle bilayers from 20°C below to 10°C above the liquid crystal-crystalline phase transition at 24°C. *Biochemistry*. 27:8261–8269.
12. Masui, T., N. Urakami, and M. Imai. 2008. Nano-meter-sized domain formation in lipid membranes observed by small angle neutron scattering. *Eur. Phys. J. E*. 27:379–389.
13. Veatch, S. L., and S. L. Keller. 2005. Seeing spots: complex phase behavior in simple membranes. *Biochim. Biophys. Acta*. 1746:172–185.
14. Nagle, J. F., and S. Tristram-Nagle. 2000. Structure of lipid bilayers. *Biochim. Biophys. Acta*. 1469:159–195.
15. Ohno, M., T. Hamada, …, M. Homma. 2009. Dynamic behavior of giant liposomes at desired osmotic pressures. *Langmuir*. 25: 11680–11685.
16. Karatekin, E., O. Sandre, …, F. Brochard-Wyart. 2003. Cascades of transient pores in giant vesicles: line tension and transport. *Biophys. J*. 84:1734–1749.
17. Rodriguez, N., S. Cribier, and F. Pincet. 2006. Transition from long- to short-lived transient pores in giant vesicles in an aqueous medium. *Phys. Rev. E Stat. Nonlin. Soft Matter Phys*. 74:061902.
18. Sandre, O., L. Moreaux, and F. Brochard-Wyart. 1999. Dynamics of transient pores in stretched vesicles. *Proc. Natl. Acad. Sci. USA*. 96:10591–10596.
19. Nomura, F., M. Nagata, …, K. Takiguchi. 2001. Capabilities of liposomes for topological transformation. *Proc. Natl. Acad. Sci. USA*. 98:2340–2345.
20. Nakano, M., M. Fukuda, …, T. Handa. 2007. Determination of interbilayer and transbilayer lipid transfers by time-resolved small-angle neutron scattering. *Phys. Rev. Lett.* 98:238101.
21. Mayor, S., J. F. Presley, and F. R. Maxfield. 1993. Sorting of membrane components from endosomes and subsequent recycling to the cell surface occurs by a bulk flow process. *J. Cell Biol.* 121:1257–1269.
22. Holthuis, J. C., and T. P. Levine. 2005. Lipid traffic: floppy drives and a superhighway. *Nat. Rev. Mol. Cell Biol.* 6:209–220.
23. Tian, A., and T. Baumgart. 2009. Sorting of lipids and proteins in membrane curvature gradients. *Biophys. J*. 96:2676–2688.
24. Genzer, J., and J. Groenewold. 2006. Soft matter with hard skin: from skin wrinkles to templating and material characterization. *Soft Matter*. 2:310–323.
25. Cerda, E., and L. Mahadevan. 2003. Geometry and physics of wrinkling. *Phys. Rev. Lett.* 90:074302.
26. Bozic, B., S. Svetina, …, R. E. Waugh. 1992. Role of lamellar membrane structure in tether formation from bilayer vesicles. *Biophys. J*. 61:963–973.

27. Taniguchi, T. 1996. Shape deformation and phase separation dynamics of two-component vesicles. *Phys. Rev. Lett.* 76:4444–4447.

28. Seifert, U. 1993. Curvature-induced lateral phase segregation in two-component vesicles. *Phys. Rev. Lett.* 70:1335–1338.

29. Kawakatsu, T., D. Andelman, …, T. Taniguchi. 1993. Phase separations and shapes of two component membranes and vesicles. I. Strong segregation limit. *J. Phys. II (France).* 3:971–997.

30. Taniguchi, T., K. Kawasaki, …, T. Kawakatsu. 1994. Phase separations and shapes of two component membranes and vesicles. II. Weak segregation limit. *J. Phys. II (France).* 4:1333–1362.

31. Lipowsky, R., and R. Dimova. 2003. Domains in membranes and vesicles. *J. Phys. Condens. Matter.* 15:S31–S45.

32. Jülicher, F., and R. Lipowsky. 1996. Shape transformations of vesicles with intramembrane domains. *Phys. Rev. E Stat. Phys. Plasmas Fluids Relat. Interdiscip. Topics.* 53:2670–2683.

33. Jülicher, F., and R. Lipowsky. 1993. Domain-induced budding of vesicles. *Phys. Rev. Lett.* 70:2964–2967.

34. Lipowsky, R. 1992. Budding of membranes induced by intramembrane domains. *J. Phys. II (France).* 2:1825–1840.

35. Sunil Kumar, P. B., G. Gompper, and R. Lipowsky. 2001. Budding dynamics of multicomponent membranes. *Phys. Rev. Lett.* 86:3911–3914.

36. Laradji, M., and P. B. Sunil Kumar. 2004. Dynamics of domain growth in self-assembled fluid vesicles. *Phys. Rev. Lett.* 93:198105.

37. Laradji, M., and P. B. Sunil Kumar. 2005. Domain growth, budding, and fission in phase-separating self-assembled fluid bilayers. *J. Chem. Phys.* 123:224902.

38. Yamamoto, S., and S. Hyodo. 2003. Budding and fission dynamics of two-component vesicles. *J. Chem. Phys.* 118:7937–7943.

39. Lim, H. W., G. M. Wortis, and M. Ranjan. 2008. Red blood cell shapes and shape transformations: Newtonian mechanics of a composite membrane. *In* Soft Matter, Vol. 4. Lipid Bilayers and Red Blood Cells. G. Gompper and M. Schick, editors. Wiley-VCH Verlag, Weinheim, Germany.